nature communications

Article

https://doi.org/10.1038/s41467-026-69239-w

Sex-specific differences in mediobasal hypothalamus in response to nutritional states

Received: 17 August 2025

Accepted: 26 January 2026

Published online: 19 February 2026

Check for updates

Jonathan C. Bean[1,8], Jinjing Jian[1,7,8], Tzu-Chiao Lu[2,3], Hailan Liu[1,7], Kristine Conde[1,7], Darah A. Threat[1], Sanika V. Jossy[1], Megan E. Burt[1], Jingjing Cheng[1,7], Yue Deng[1,7], Xing Fang[1], Xiaoyu Geng[1], Junying Han[1], Yongxiang Li[1,7], Hesong Liu[1], Qingzhuo Liu[1,7], Yutian Liu[1,7], Yuhan Shi[1], Longlong Tu[1,7], Mengjie Wang[1,7], Xu Xu[1], Yuxue Yang[1,7], Meng Yu[1], Xinming Liu[1,7], Meixin Sun[1,7], Fuhui Wang[1,7], Olivia Z. Ginnard[1], Yongjie Yang[1,7], Yang He[4], Chunmei Wang[1], Yanyan Qi[2,3], Hongjie Li[2,3] ✉ & Yong Xu[1,5,6,7] ✉

The arcuate nucleus of the hypothalamus plays a central role in sensing and integrating nutritional, hormonal, and neural signals that regulate feeding, energy homeostasis, growth, and reproduction, all of which show pronounced sex differences. However, the cellular mechanisms underlying these responses remain poorly understood. We performed snRNA-seq of the mediobasal hypothalamus, focusing on the arcuate nucleus, in female and male mice under different nutritional states. Analysis of 42 cell types revealed that Agrp neurons were most sensitive to nutritional changes, dopaminergic neurons showed strong sex-specific differences, and KNDy neurons were highly responsive to both sex and nutrition. Pomc neurons displayed moderate nutritional sensitivity. Most glial populations were stable, although microglia and oligodendrocytes showed moderate variation. Cell–cell communication analysis identified neurotrophic factor signaling as a key pathway regulated by sex and nutrition. This study represents a major effort to comprehensively characterize sex-specific differences in arcuate nucleus response across nutritional conditions.

Worldwide obesity has been steadily increasing since the mid 1970s with more than 13% of adults categorized as obese in 2016[1]. In the United States obesity has become an epidemic with greater than 40% of adults categorized as obese in 2020[2]. Obesity increases the risk for many negative health outcomes, including type 2 diabetes, cardiovascular disease, and nonalcoholic fatty liver disease[1–3].

Sex differences are evident in metabolic homeostasis. Historically, females experienced higher rates of obesity than males, although this difference may be diminishing in the Western world[1,2]. Adipose tissue distribution varies between the sexes: females store more subcutaneous fat, while males store more visceral fat. Excessive visceral fat is associated with worse health outcomes[4,5], and females are protected

[1]USDA/ARS Children's Nutrition Research Center, Department of Pediatrics, Baylor College of Medicine, Houston, TX, USA. [2]Huffington Center on Aging, Baylor College of Medicine, Houston, TX, USA. [3]Department of Molecular and Human Genetics, Baylor College of Medicine, Houston, TX, USA. [4]Jan and Dan Duncan Neurological Research Institute, Texas Children Hospital, Houston, TX, USA. [5]Department of Molecular and Cellular Biology, Baylor College of Medicine, Houston, TX, USA. [6]Department of Medicine, Baylor College of Medicine, Houston, TX, USA. [7]Present address: Center for Molecular Psychiatry, Department of Psychiatry & Behavioral Neurosciences, Morsani College of Medicine, University of South Florida, Tampa, FL, USA. [8]These authors contributed equally: Jonathan C. Bean, Jinjing Jian. ✉e-mail: hongjie.li@bcm.edu; yongxu@usf.edu

from these before menopause[6]. Interestingly, deletion of estrogen receptor-α (encoded by the *Esr1* gene) from the ventromedial hypothalamus (VMH) caused female mice to accumulate visceral fat like male mice[7], demonstrating the significant role of specific brain regions in regulating metabolic homeostasis.

The arcuate nucleus of the hypothalamus (ARH) is located beside the third ventricle and above the median eminence (ME), where the blood brain barrier is more permeable[8]. This positioning enables the ARH to receive peripheral paracrine signals from adipose, liver, and pancreas[9,10]. Seminal studies by Camus and Roussy followed by Bailey and Bremer established that the infundibulo-tuberal region, including ARH, exerts control over homeostatic feeding, in the early 20th century[11]. Manipulations of neural circuits in the ARH have demonstrated its critical role in feeding behavior. Chemogenetically activating agouti-related peptide (Agrp) neurons resulted in hyperphagia[12], as did optogenetically activating tyrosine hydroxylase (Th)-expressing neurons[13]. A rapid decrease in feeding was seen when oxytocin receptor-expressing neurons were activated via chemo or optogenetics[14]. Additionally, a decrease in feeding was observed that took sustained activation of pro-opiomelanocortin (Pomc) neurons via chemogenetics[15]. The ARH is also home to kisspeptin 1 (Kiss1) neurons responsible for controlling fertility and neurons responsible for controlling growth hormone release[16,17].

These findings highlight the remarkable heterogeneity of ARH neurons, both in their transcriptomic profiles and functional diversity. While previous research has explored the ARH's role in metabolic regulation, most studies have focused on responses to nutritional challenges, with limited attention to sex-specific differences[18–20].

In this study, we comprehensively investigate sex-specific cellular responses in the mediobasal hypothalamus (MBH) with a focus on the ARH under varying nutritional states, using single-nucleus RNA sequencing (snRNA-seq). This approach allows us to capture the transcriptional landscape at a cellular resolution. We identified pronounced sex differences in Kiss1-Neurokinin B-Dynorphin (KNDy) neurons and moderate differences in dopamine (DA) neurons, highlighting distinct roles these cells may play in male and female energy homeostasis. Additionally, we observed substantial nutritional state-dependent changes in Agrp and KNDy neurons, with Pomc neurons, microglia, and oligodendrocytes showing moderate responses. Our findings offer a perspective on how sex and nutritional state interact at the cellular level within the ARH, paving the way for more targeted and effective interventions for metabolic disorders that account for these critical biological differences.

Results

Single-nucleus transcriptomes for the ARH of female and male mice in different nutritional states

In order to investigate sex differences in nutritional state response, we performed snRNA-seq on the MBH with a focus on ARH tissue from female and male mice that were either fed *ad libitum* or fasted for 28 h (Fig. 1a, b; Supplementary Fig. 1a, b). In our study, we leveraged mice natural nocturnal behavior, euthanizing them 4 h into their dark cycle when they are most active (Supplementary Fig. 1a). We did this to ensure the *ad lib* fed mice were in a well fed state and the fasted mice would be in a state of high food craving. To attain a high-quality analysis of sex by nutritional state interactive characteristics, we profiled 36 mice, 18 males, and 18 females (Fig. 1a). After standard preprocessing steps, such as removing ambient RNAs and doublets[21–25] (Supplementary Fig. 1c), we got 93,265 high-quality nuclei in total (Fig. 1c). We achieved near equal sequencing depth and feature detection across conditions with around 5700 mean unique molecules (UMIs), and 2900 mean unique genes detected per nucleus with a minimal number of reads assigned to hemoglobin, ribosomal binding proteins, and mitochondrial mRNA (Supplementary Fig. 1d).

Next, we performed principal component analysis (PCA) followed by t-distributed stochastic neighbor embedding (tSNE) dimensionality reduction for visualization. K-nearest neighbors clustering calculations were performed based on the first 30 PCs to identify cell clusters. Our analyses identified 42 distinct cell-types (31 types of neurons and 11 types of glia) (Fig. 1d; Supplementary Figs. 2, 3). We found that nuclei from both sexes under both nutritional states mapped similarly in tSNE space (Fig. 1c), suggesting cell-types do not change across nutritional states or differ between the sexes. We also confirmed that there were no major batch effects (Supplementary Fig. 1e). Overall, 65,014 neurons and 28,251 glia were obtained from the MBH region, including 41,622 neurons representing all neuronal types in ARH (Fig. 1d). To ensure that observed transcriptional differences reflect true biological variation rather than technical artifacts, we performed the RPCA-based integration within the Agrp neurons and KNDy neurons separately across different batches. After integration, the tSNE space embeddings showed well-mixed distributions of cells from different batches (Figs. 2a, 4a, Supplementary Figs. 5b,12b). In addition, integration of our neuronal dataset with the Campbell et al.[18] dataset (neurons only) demonstrated high transcriptomic similarity between datasets (Supplementary Fig. 4a). Most cell types showed strong alignment across both datasets, and only minor differences in cell subtype labeling were observed (Supplementary Fig. 4b). These results support the robustness of our integration approach and validate the accuracy of our cell type annotations for downstream analyses. Our annotation was also aided by annotation from the Allen brain atlas[26].

We next examined which cell-types' transcriptomes differed either across sex or nutritional state. Here we define differential expression (DE) as: greater than 25% nuclei of at least one condition expressed the gene, the difference in expression between the groups larger than 1.25-fold, and the adjusted p-value less than 0.05. We used model-based analysis of single-cell transcriptomics (MAST) as our statistical test using sample ID as a latent variable[26]. Six of the 10 most dynamic cell-types were ARH neurons (Fig. 1e), with the other four being Oligodendrocytes, α-Tanycytes, β-Tanycytes and a large cluster MM.01. It was possible that larger cell-type clusters appeared more dynamic (ie more DE genes) because they had more statistical power to detect these changes. In order to control this possibility, we performed down-sampling to 200 nuclei per condition per cell-type and repeated our DE analyses. Controlling for cluster size did highlight some smaller clusters as being more dynamic than they initially appeared (eg Microglia, DA, and Coch/Slc18a2); however larger clusters that appeared dynamic in absolute terms remained dynamic after controlling for size (eg Agrp, and KNDy neurons) (Fig. 1f).

Summary of cell-types that are sensitive to nutritional state in a sex-specific manner

Overall, more nutritionally regulated DE genes (DEGs) were observed in female mice. We saw both male and female mice had the most nutritionally regulated DEGs for the Agrp cluster. Other clusters that saw dynamic responses to nutrition for both sexes were: Pomc, Sst/Unc13c, Lamp5/Npy5r, and Ghrh/Chat neurons. Strikingly, KNDy neurons appeared very sensitive to nutritional state in females but not in males. To a lesser extent DA neurons and related cluster Coch2/Slc18a2 also responded to nutritional state in females but not in males (Fig. 1e). Relatedly, when comparing across sexes within nutritional state, KNDy neurons showed the most sexual dimorphism followed by DA neurons. Of note, Lamp5/Npy5r, Ghrh/Chat, and Coch2/Slc18a2 neurons also showed sexual dimorphism each with numerous DEGs between the sexes (Fig. 1e). Strikingly, almost all sexually regulated DEGs were on autosomes and not on sex chromosomes (X and Y) (Fig. 1e inset). The same patterns hold true after controlling for cluster size (Fig. 1f). Two of the most dynamic glia-types were oligodendrocytes and microglia (Fig. 1f).

https://doi.org/10.1038/s41467-026-69239-w

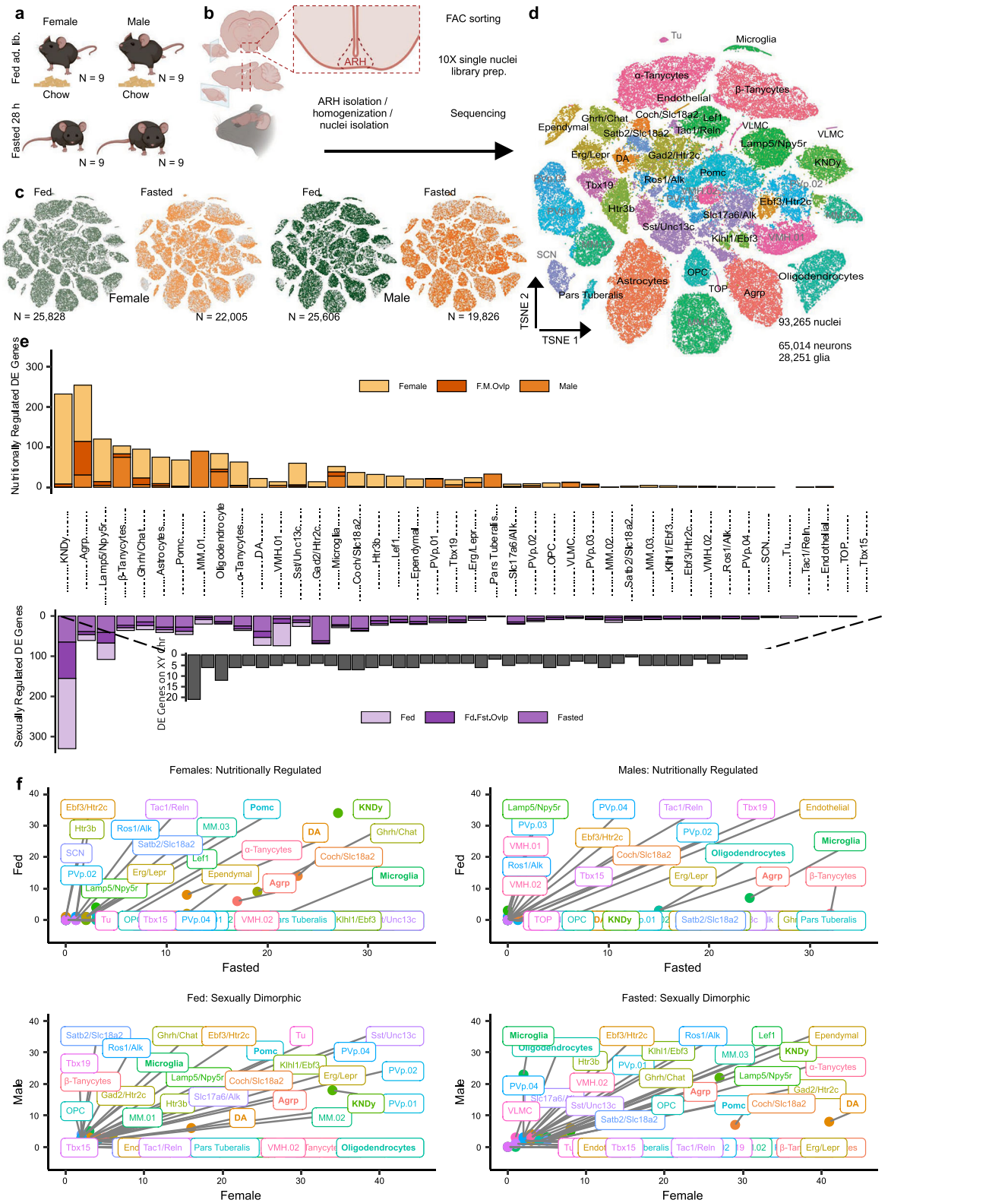

Fig. 1 | Design and scope. a Diagram depicting study design. Female and male mice in either ad lib fed or fasted conditions were used for this study. **b** Flow chart depicting the collection of ARH brain tissue, nuclei isolation, single nuclei library preparation, and sequencing. **a**, **b** prepared using BioRender. **c** Nuclei plotted in tSNE space split across conditions. **d** Nuclei plotted in tSNE space color coded by cell-type. **e** Number of differentially expressed genes (DE) for comparisons across nutritional conditions in orange and across sex in purple. DE genes defined as >25% of cells in at least one condition express the gene, >25% difference between conditions, and adjusted p-value < 0.05 after MAST test with Bonferroni correction. **f** Number of DE genes for clusters when downsampled to 200 nuclei per condition. Source data are provided as a Source Data file. F.M.Ovlp female and male overlap, Fd.Fst.Ovlp fed and fasted overlap, MM medial mammillary nucleus, DA, dopamine; PVp, posterior periventricular nucleus; OPC, Oligodendrocyte precursor cells; SCN, suprachiasmatic nucleus, VLMC vascular leptomeningeal cells, Tu olfactory tubercle, TOP true committed oligodendrocyte progenitor cell, TSNE t-distributed stochastic neighbor embedding. Illustrations in (**a**, **b**) were created in BioRender. Jian, J. (2026) https://BioRender.com/0cfg9ic.

https://doi.org/10.1038/s41467-026-69239-w

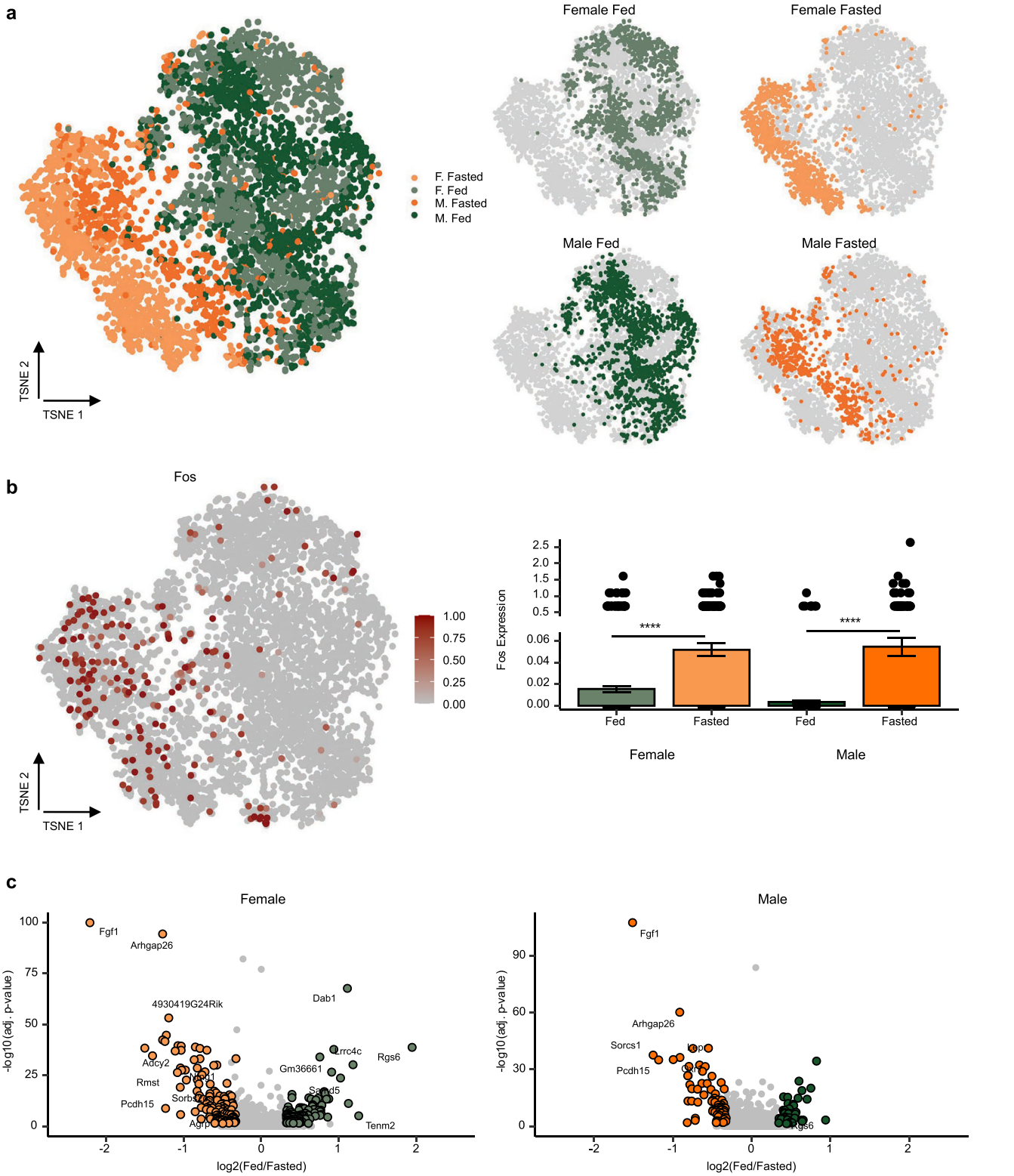

Fig. 2 | Agrp neurons are nutritionally regulated. a Agrp neurons plotted in tSNE space, color coded by condition, plotted intermixed, left, or separately, right. **b** *Fos* expression in Agrp neurons. Left: *Fos* feature plot showing normalized expression levels across Agrp neurons. Right: Histogram of *Fos* expression showing mean ± SEM ($n = 3$ biological replicates per condition). Statistical significance was determined using the two-sided Wilcoxon rank-sum test with Bonferroni correction; **** = adjusted $p = 9.59$ e-06 and $p = 8.74$ e-15 respectively. **c** Volcano plots with DE genes, when comparing fed and fasted, plotted in color with females on the left and males on the right. Statistical significance was determined using MAST with Bonferroni correction. M male, F female, TSNE t-distributed stochastic neighbor embedding.

Next, we will focus on 4 neuron-types (Agrp, KNDy, DA, and Pomc) and 2 glia-types (oligodendrocytes and microglia) that show the most profound changes.

Agrp neurons are nutritionally dynamic

Agrp neurons are crucial for the control of feeding behavior. Ablation of Agrp neurons from adult mice causes rapid starvation, while activation causes rapid food consumption[12,27]. In our data, Agrp cluster exhibited approximately 240 nutritionally regulated DEGs (adjusted $p < 0.05$), showing the strongest transcriptional response to nutritional state among all clusters (Fig. 1e, f). To perform more detailed analysis, we isolated Agrp neurons and reclustered them. To ensure that observed transcriptional differences reflected true biological variation rather than technical artifacts, we performed RPCA-based integration within the Agrp neurons across different batches. After integration, the tSNE space embeddings showed well-mixed distributions of cells from different batches (Fig. 2a; Supplementary Fig. 5b). Interestingly, they largely segregated by nutritional state (Fig. 2a) and to a lesser extent by sex. Analysis of *Fos* expression indicates that Agrp neurons are activated by fasting in both females and males (Fig. 2b). DE analyses revealed a large number of nutritionally regulated DEGs in both sexes, with 254 unique DEGs (adjusted $p < 0.05$) identified across female and male Agrp neurons, and 61 DEGs showing sex-dependent expression differences (Supplementary Data 12). Representative nutritionally regulated genes, such as *Fgf1* and *Rgs6*, were further validated by RNAscope (Fig. 2c; Supplementary Figs. 6, 7). We then performed gene ontology molecular function (GO:MF) for the DEGs. In females, PDZ binding domain was suppressed by fasting, while GTPase activity and cAMP binding were induced by fasting (Supplementary Data 1). While Agrp neurons were sexually dimorphic, the extent was lesser in degree than the nutritional regulation (Supplementary Fig. 5a; Supplementary Data 12). To evaluate nutritional and sex effects within potential Agrp sub-clusters, we performed co-embedding analyses for Agrp neurons populations with the Campbell reference dataset[18], transferred subcluster-level annotations to corresponding cells, and validated these assignments by examining known marker expression within each sub-cluster (Supplementary Fig. 8a, b). Analyses stratified by sex and nutritional state within the annotated sub-clusters recapitulated the patterns observed at the major cluster level, indicating that our conclusions are robust to sub-cluster resolution (Supplementary Figs. 8, 9). In summary, Agrp neurons are highly sensitive to nutritional state and moderately sexually dimorphic.

Pomc neurons are nutritionally dynamic

Related Pomc neurons are also crucial for the control of feeding behavior. Although not one of the top most dynamic clusters, Pomc neurons still exhibited 68 nutritionally regulated DEGs across both sexes and 46 DEGs showing sex-dependent expression differences (adjusted $p < 0.05$, Supplementary Data 13). After reclustering Pomc neurons, they too segregated by nutritional state (Fig. 3a). We observed more *Fos* expression in the fed state for both sexes; however, only males were statistically significant (Fig. 3b). Performing GO:MF on DEGs revealed that cAMP binding was suppressed by a fast in females while voltage-gated potassium channel activity was induced by a fast in females (Supplementary Data 2). Growth hormone receptor activity was higher in fed males than females, while glutamate receptor activity was higher in fasted females than males (Supplementary Data 3). To evaluate nutritional and sex effects at sub-cluster resolution within Pomc neurons, we co-embedded our dataset with the Campbell reference dataset[18], transferred three sub-cluster annotations (Pomc/Anxa2, Pomc/Glipr1, Pomc/Ttr) to the corresponding cells, and validated these assignments by examining canonical marker expression for each sub-cluster (Supplementary Figs. 10 a, b). Stratified analyses by sex and nutritional state within the annotated sub-clusters recapitulated the patterns observed at the major-cluster level, indicating that our conclusions are robust at subcluster resolution (Supplementary Fig. 10, 11).

KNDy neurons are nutritionally regulated in females and are sexually dimorphic

KNDy neurons are responsible for controlling the pulsatile release of gonadotropin-releasing hormone (GnRH) and ultimately FSH and LH[16]. After sub-clustering, we also performed RPCA-based integration analysis within the KNDy neurons across different batches. After integration, the tSNE space embeddings showed well-mixed distributions of cells from different batches. Notably, KNDy neurons revealed female cells in the fed state and fasted state occupied distinct locations on the tSNE map, while male cells of both the fed and fasted states were intermingled and distinct from female cells (Fig. 4a). This is reflective of the large number of sexually dimorphic DEGs we saw (330 DEGs, adjusted $p < 0.05$), as well as, the large number of nutritionally regulated DEGs we saw in females (231 DEGs, adjusted $p < 0.05$) (Figs. 1e, f, 4b, c, Supplementary Data 14). Analysis of *Fos* expression did not reveal any activity in any state for both sexes (Supplementary Fig. 12a). RNAscope failed to confirm DE gene *Cntn5* but was able to confirm DE gene *Tmem266* (Supplementary Figs. 13, 14). Genes suppressed by fasting in females were related to cAMP binding, while genes induced by fasting were related to potassium channel regulator activity and glutamate receptor activity (Supplementary Data 4). Among sexually dimorphic genes, females had higher expression of genes related to nuclear receptor activity and transcription coregulator binding while males had higher expression of genes related to nitric-oxide synthase binding, in the fed condition. In the fasting condition, females had higher expression of genes related to calmodulin binding and males had higher expression of genes related to extracellular matrix structural constituent conferring tensile strength (Supplementary Data 5). To summarize, KNDy neurons are both highly sexually dimorphic, as well as, highly sensitive to nutritional state.

DA neurons are sexually dimorphic

DA neurons in the ARH are best known for their ability to inhibit prolactin[28]. When sub-clustering DA neurons, female and male neurons occupy different areas, indicating there are significant sex-related differences. DE analysis also revealed 73 sex-dependent DEGs (adjusted $p < 0.05$) (Supplementary Data 15). Although less evident, nutritional state also influenced the transcriptional profiles of DA neurons (22 DEGs, adjusted $p < 0.05$), as reflected by subtle differences in their tSNE distribution (Fig. 5a, Supplementary Data 15). Analysis of *Fos* expression indicated that female DA neurons may be active during the fed state, while male DA neurons remain inactive at both fed and fasted states (Fig. 5b). Many sexually DEGs were present in both fed and fasted conditions (Fig. 5c, Supplementary Data 15). Females had higher expression of genes related to netrin receptor activity in both fed and fasted conditions and higher expression of neurotrophin binding genes in the fasted condition (Supplementary Data 6, 7). Females also demonstrated some nutritional regulation of genes in dopamine neurons while males show minimal changes (Supplementary Fig. 15, Supplementary Data 15). In all, dopamine neurons are highly sexually dimorphic, and show moderate nutritional sensitivity in females.

To evaluate neuronal activation beyond the reliance on *Fos* alone, we examined the expression of 44 reported immediate early genes (IEGs) in DA neurons across different sex and nutritional conditions[29]. Overall, the expression of these IEGs was low across all groups, as shown in the heatmap (Supplementary Fig. 20a). However, several genes including *Fos* and *Nr4a1* were detectable and showed a pattern of increased expression in the fed state, particularly in females (Supplementary Fig. 20a). DE analysis revealed that *Fos* and *Nr4a1* were significantly upregulated in female fed condition compared to male fed counterparts, with average log2 fold changes of 9.38 and 5.74 respectively (adjusted $p < 0.05$) (Supplementary

https://doi.org/10.1038/s41467-026-69239-w

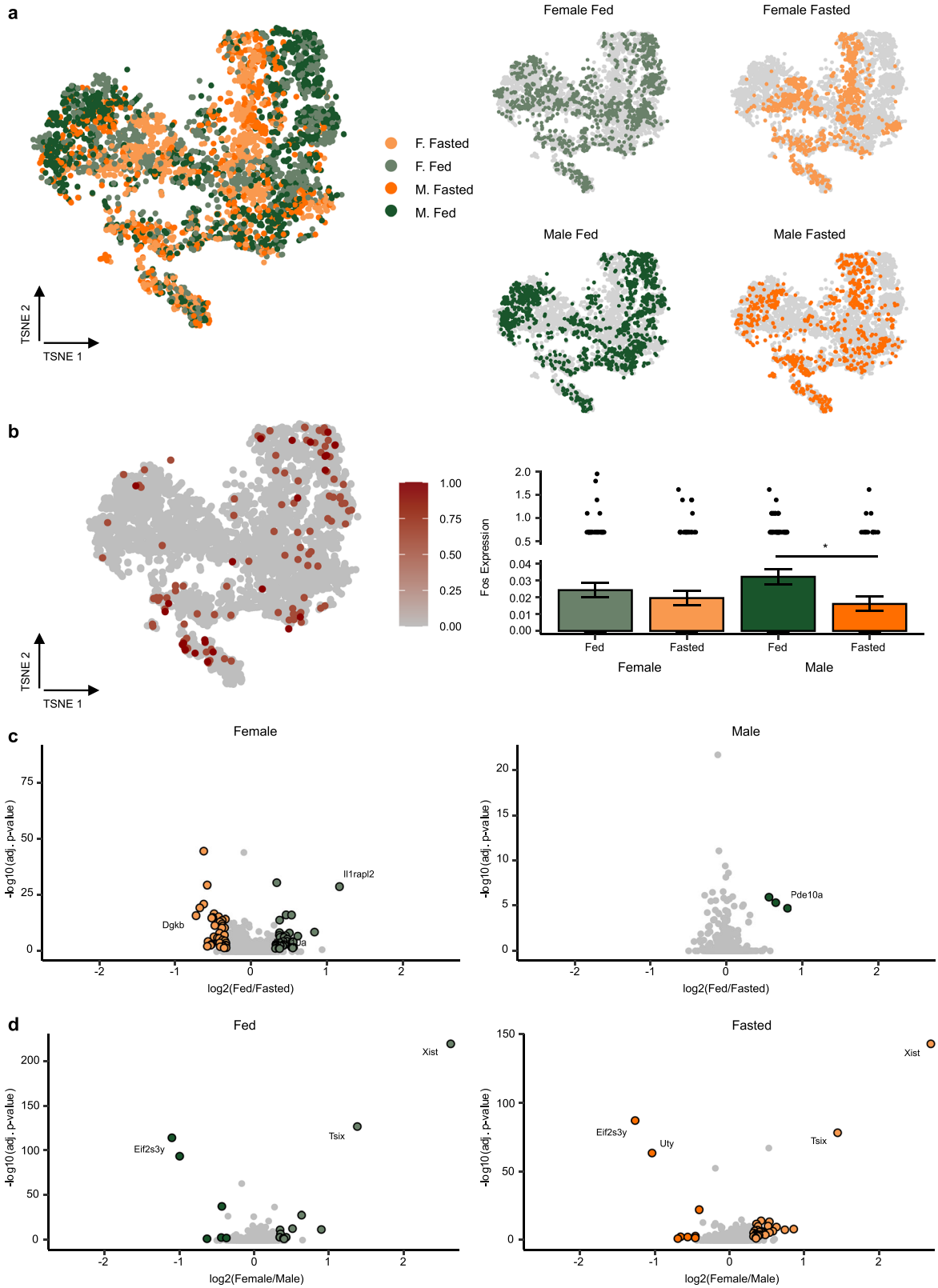

Fig. 3 | Pomc neurons are nutritionally regulated. a Pomc neurons plotted in tSNE space, color coded by condition, plotted intermixed, left, or separately, right. **b** *Fos* expression in Pomc neurons. Left: *Fos* feature plot showing normalized expression levels across Pomc neurons. Right: Histogram of *Fos* expression showing mean ± SEM ($n = 3$ biological replicates per condition). Statistical significance was determined using the two-sided Wilcoxon rank-sum test with Bonferroni correction; * = adjusted $p = 0.0121$, n.s. = not significant. **c** Volcano plots with DE genes, when comparing fed and fasted, plotted in color with females on the top left and males on the top right. **d** Volcano plots with DE genes, when comparing females vs males in the fed condition bottom left and fasted condition bottom right. **c**, **d** Statistical significance was determined using MAST with Bonferroni correction. M male, F female, TSNE t-distributed stochastic neighbor embedding.

https://doi.org/10.1038/s41467-026-69239-w

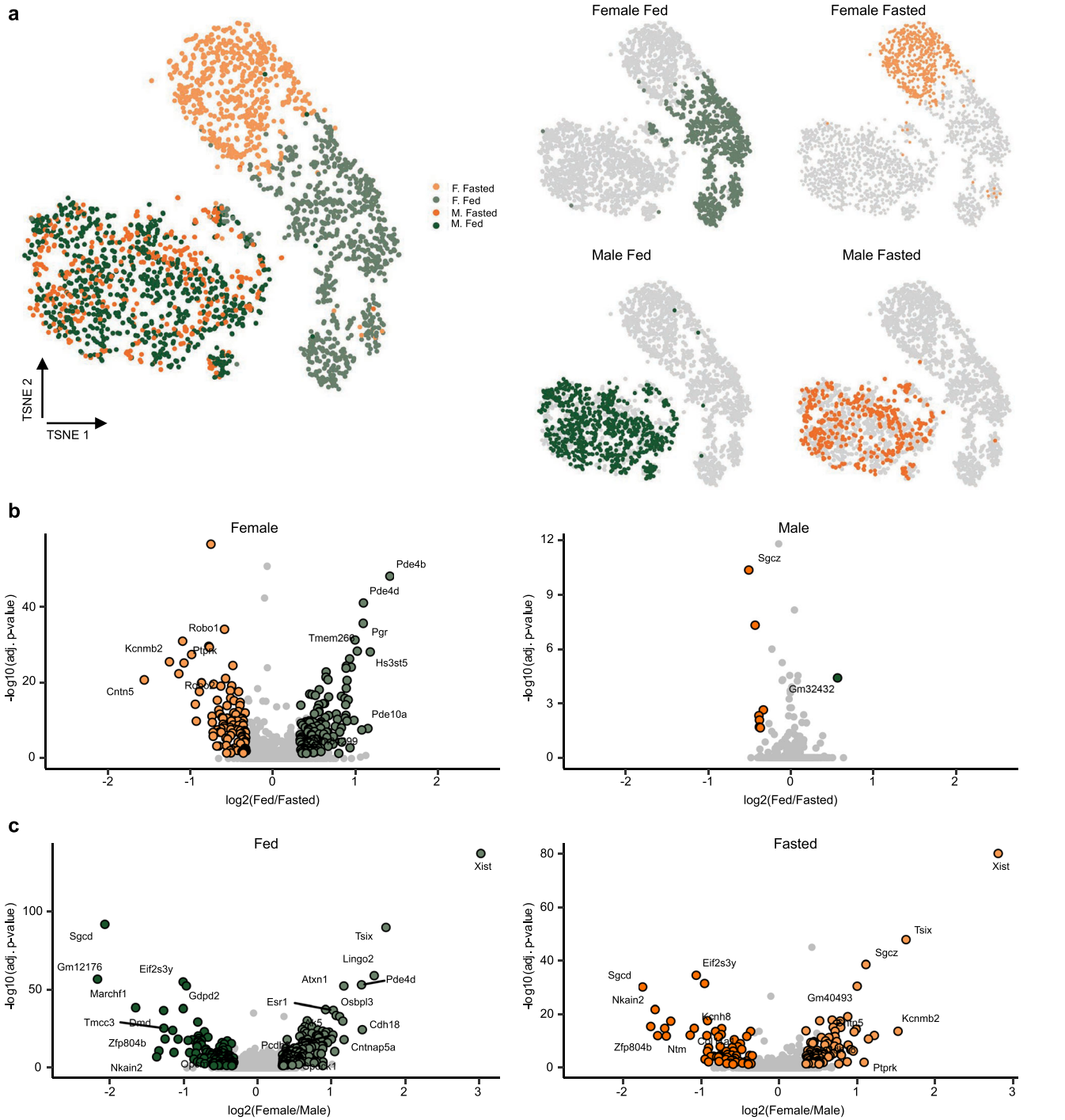

Fig. 4 | KNDy neurons nutritionally regulated in females but not males. a KNDy neurons in tSNE space color coded by sex and nutritional state plotted together, left, or separately, right. **b** Volcano plots comparing fed and fasted in females, left, or males, right. DE genes plotted in color. **c** Volcano plots comparing females vs males in the fed condition bottom left and fasted condition bottom right. **b**, **c** Statistical significance was determined using MAST with Bonferroni correction. M male, F female, TSNE t-distributed stochastic neighbor embedding.

Fig. 20b). These findings suggest that *Fos* exhibited the most robust and consistent induction among these IEGs, characterized by both high expression magnitude and pronounced sensitivity to sex and nutritional conditions.

Microglia and oligodendrocytes are moderately regulated by nutritional state

Microglia, the brain's innate immune cells, demonstrate a surprisingly stable population despite their inherent dynamic feature under different conditions, such as aging and neurodegeneration[30]. Sub-clustering analysis showed that neither sex nor nutritional state defined clear clustering patterns (Fig. S12a). Analysis of *Fos* expression could not reveal any activity (Supplementary Fig. 16b). However, DE analysis identified 52 nutritionally regulated DEGs (adjusted $p < 0.05$), particularly in females (Supplementary Fig. 16c, Supplementary Data 16), although sexually dimorphic DEGs remained minimal (29 DEGs, adjusted $p < 0.05$) (Supplementary Fig. 16d, Supplementary Data 16). Notably, fasting prominently upregulated cytoskeletal

https://doi.org/10.1038/s41467-026-69239-w

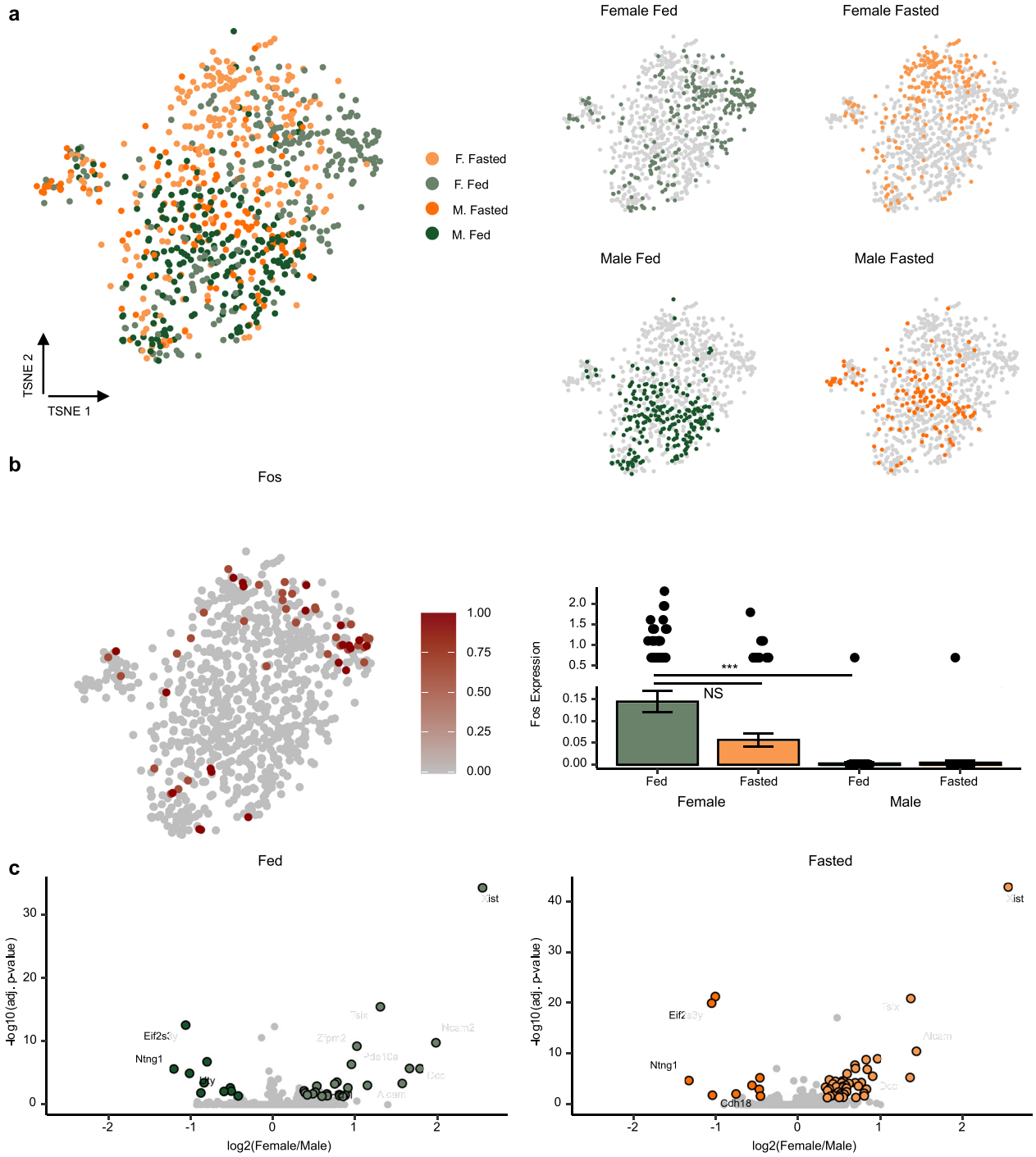

Fig. 5 | Dopamine neurons are sexually dimorphic. a DA neurons in tSNE space color coded by sex and nutritional state plotted together, left, or separately, right. **b** *Fos* expression in DA neurons. Left: *Fos* feature plot showing normalized expression levels across DA neurons. Right: Histogram of *Fos* expression showing mean ± SEM ($n = 3$ biological replicates per condition). Statistical significance was determined using the two-sided Wilcoxon rank-sum test with Bonferroni correction; *** = adjusted $p = 0.0003$, n.s. = not significant. **c** Volcano plots comparing females and males in either fed, left, or fasted, right, conditions. Statistical significance was determined using MAST with Bonferroni correction. M male, F female, TSNE t-distributed stochastic neighbor embedding, NS not significant.

protein binding in females and transmitter-gated channel activity in males (Supplementary Data 8, 9), suggesting a nutritional influence on microglial functionality.

Oligodendrocytes, the architects of myelination, exhibit a stronger effect. Their sub-clustering pattern in tSNE space appears to be nutrition-driven (Supplementary Fig. 17a). *Fos* analysis could not reveal any activity in oligodendrocytes (Supplementary Fig. 17b). Nutritionally regulated DEGs were abundant across both sexes, with 84 genes (adjusted $p < 0.05$) identified as nutritionally responsive and 20 genes showing sex-dependent expression differences (adjusted $p < 0.05$) (Supplementary Fig. 17c, d, Supplementary Data 17). Interestingly, fasting conditions led to an shared increase in ion channel regulator activity genes across both males and females (Supplementary Data 10, 11), similar to microglial responses.

Overall, despite their known responsiveness in neurodegenerative and other neurological disease conditions[30,31], glial cells—both microglia and oligodendrocytes—display a relative stability across sexes and nutritional states in this study. This unexpected resilience may reflect a tightly regulated homeostatic mechanism in these glial cells, while external nutritional fluctuations primarily affect neuronal types in ARH.

Cell-cell communication analysis reveals trophic factors as a major target of nutritional and sexual regulation

Many of the GO:MF terms generated by the DEGs from comparing across conditions were related to cell signaling. In order to investigate this further, we deployed a cell-cell communication analysis using Cellchat (Figs. 6, 7)[32].

Using joint manifold learning we compared fed and fasted states in male and female mice. This identified four distinct signaling pathways for both sexes, although the way they clustered in manifold space was vastly different (Fig. 6a, b). When comparing fed and fasted female mice, signaling pathways including Tgfβ, Ghrh, and Vegf, were weighted more heavily in the fed condition, while Fgf, Tsh, and Npy were weighted more heavily in the fasted condition (Fig. 6c). When comparing fed and fasted male mice, Pacap, Dheas, and testosterone were weighted more heavily in the fed condition, whereas, Vegf, Npy, and Gas were weighted more heavily in the fasted condition (Fig. 6d). Focusing on nutritional regulation of ligands we saw that *Fgf1* was suppressed by fasting in Pomc neurons while being induced in Agrp neurons in females. Females also saw *Nrg3* induced by fasting in Agrp neurons. Males saw an increase in *Lrrc4c* in microglia during fasting (Fig. 6e). Shifting our focus to receptors regulated by nutritional state revealed *Erbb4* was suppressed by a fast in both males and females in Agrp neurons. In addition, *Erbb4* was suppressed by fasting in KNDy neurons in females but not males. Females saw *Robo1* and *Robo2* induced by fasting in KNDy neurons (Fig. 6f).

Next, we examined differences between female and male mice in either the fed or the fasted condition. We again saw clustering of four distinct signaling pathways for both fed and fasted conditions but with vastly different clustering in the manifold space (Fig. 7a, b). When comparing female and male mice in the fed condition, signaling pathways including Psap, Csf, and Tac were weighted more heavily toward females, while Dopamine, Ephb and Pdgf were weighted more heavily in male mice (Fig. 7c). When comparing female and male mice in the fasted condition, signaling pathways including Pacap, Dheas, and Tac were weighted more heavily in females, while Dopamine, Ghrh, and Gas were weighted more heavily in males (Fig. 7d). We next examined sexually dimorphic ligand and receptor pairs. *Nrg3* was greater in female mice in KNDy neurons in both the fed and fasted states, while *Nrg3* was greater in DA neurons in males in the fed state (Fig. 7e). Females saw a greater level of expression of *Robo1* in KNDy neurons in the fasted state (Fig. 7f).

To further support these findings, we used NicheNet to validate the predicted ligand–receptor interactions identified by Cellchat. For example, the NicheNet validation result confirmed that *Nrg3* had strong ligand activity and was predicted to regulate downstream target genes, such as *Erbb4* in Agrp neurons, in agreement with our original Cellchat predictions (Fig. 6e, f). In addition, *Nrg3* was highly expressed in Agrp neurons of fasted female mice (Supplementary Fig. 18a, d), suggesting that Agrp neurons may also function as sender cells, with *Nrg3* potentially acting on target genes in other cell types. Similarly, in KNDy neurons, NicheNet identified *Nrg3*, *Nrg1*, and *Slit2* as active ligands derived from various sender populations, including endothelial and Sst/Unc13c neurons. *Nrg3* showed strong regulatory potential for *Erbb4*, while *Slit2* was predicted to act on *Robo1* and *Gpc1*, supporting a Slit–Robo signaling axis modulated by fasting in females (Fig. 6e, f; Supplementary Fig. 18b, d). Our Cellchat analysis identified *Slit2*, *Lrfn5*, *Fgf1*, and *Mag* as potential active ligands in oligodendrocytes. NicheNet validation indicated that these ligands, expressed by Ghrh/Chat neurons and endothelial cells, demonstrated varying degrees of ligand activity. Notably, *Slit2* showed strong prior interaction potential with *Robo2*; *Lrfn5* was linked to receptors *Ptprs* and *Ptprd*; and *Fgf1* showed potential to regulate *Fgfr2* in oligodendrocytes. (Fig. 6e, f; Supplementary Fig. 18c, d). Together, these NicheNet validation results provide further support for the ligand–receptor interactions inferred by CellChat.

In summary, neurotrophic factors are induced in neurons that are also activated during fasting like Agrp neurons and suppressed by fasting in neurons suppressed or likely suppressed by fasting like Pomc neurons. Neurotrophic factors were expressed higher in females in neurons that may play a larger role in females, like KNDy and dopamine neurons. Neurotrophic receptors saw the opposite regulation that neurotrophic factors saw.

Co-expression network analysis reveals nutrient- and sex-responsive gene modules

To investigate potential coordinated gene expression in Agrp neurons, we applied hdWGCNA and identified 13 gene co-expression modules (Supplementary Fig. 19a). Differential module eigengene (DME) analysis revealed that several modules were significantly regulated by nutritional state and/or sex (Supplementary Fig. 19g). For example, Module 4 was upregulated in fasted females and enriched for genes involved in inhibitory synapse assembly, cAMP binding, postsynaptic membrane potential regulation, and sympathetic nervous system development (Supplementary Fig. 19b, c). The hub gene *Nrg3*, previously predicted as a fasting-induced ligand in Agrp neurons, was also present in this module. Another nutrient- and sex-responsive module, Module 6 (Agrp_M6), was enriched for terms, such as feeding behavior, signal transduction, and neuron projection (Supplementary Fig. 19d, e). Functional annotation across all modules further revealed widespread enrichment in biological processes related to synaptic function, energy metabolism, and behavioral regulation (Supplementary Fig. 19f).

DME analysis further revealed condition-specific module regulation patterns across sex and nutritional states (Supplementary Fig. 19g). Specifically, Modules M4, M6, and M10 were upregulated in fasted females, while Modules M5 and M11 were enriched in fed females. In males, Modules M10 and M6 showed higher expression under fasting, whereas Modules M1 and M5 were more active in the fed state. These findings underscore the sexually dimorphic and nutrient-sensitive nature of co-expression programs in Agrp neurons.

Discussion

When food is not available, animals need to suppress energy expenditure which preserves energy storage; animals also need to promote counterregulatory responses in order to avoid severe hypoglycemia. Meanwhile, animals need to overcome anxiety and fear to seek food which is often associated with danger[33–36]. All these physiological and behavioral adaptations to survive food deprivation are coordinated through complex neuroendocrine mechanisms which differ between males and females. Here we delineate the extent of sex differences in the cells of the ARH under different nutritional states. We found major sex differences in KNDy neurons as well as moderate sex differences in DA neurons in the ARH. Notably, the majority of genes with sexually dimorphic expression patterns are located on the autosomes. Major nutritional state differences were noted in Agrp and KNDy neurons while moderate nutritional state differences were found in Pomc neurons, microglia and oligodendrocytes.

Agrp neurons in the ARH release Agrp, Npy, and GABA onto upstream Mc4r neurons in the PVH inhibiting Mc4r neurons and promoting feeding behavior[32–34]. Agrp neurons in the ARH are activated by ghrelin and asprosin during food deprivation and suppressed by leptin when animals are well fed[35–37]. Agrp neuron activity is mostly silent

https://doi.org/10.1038/s41467-026-69239-w

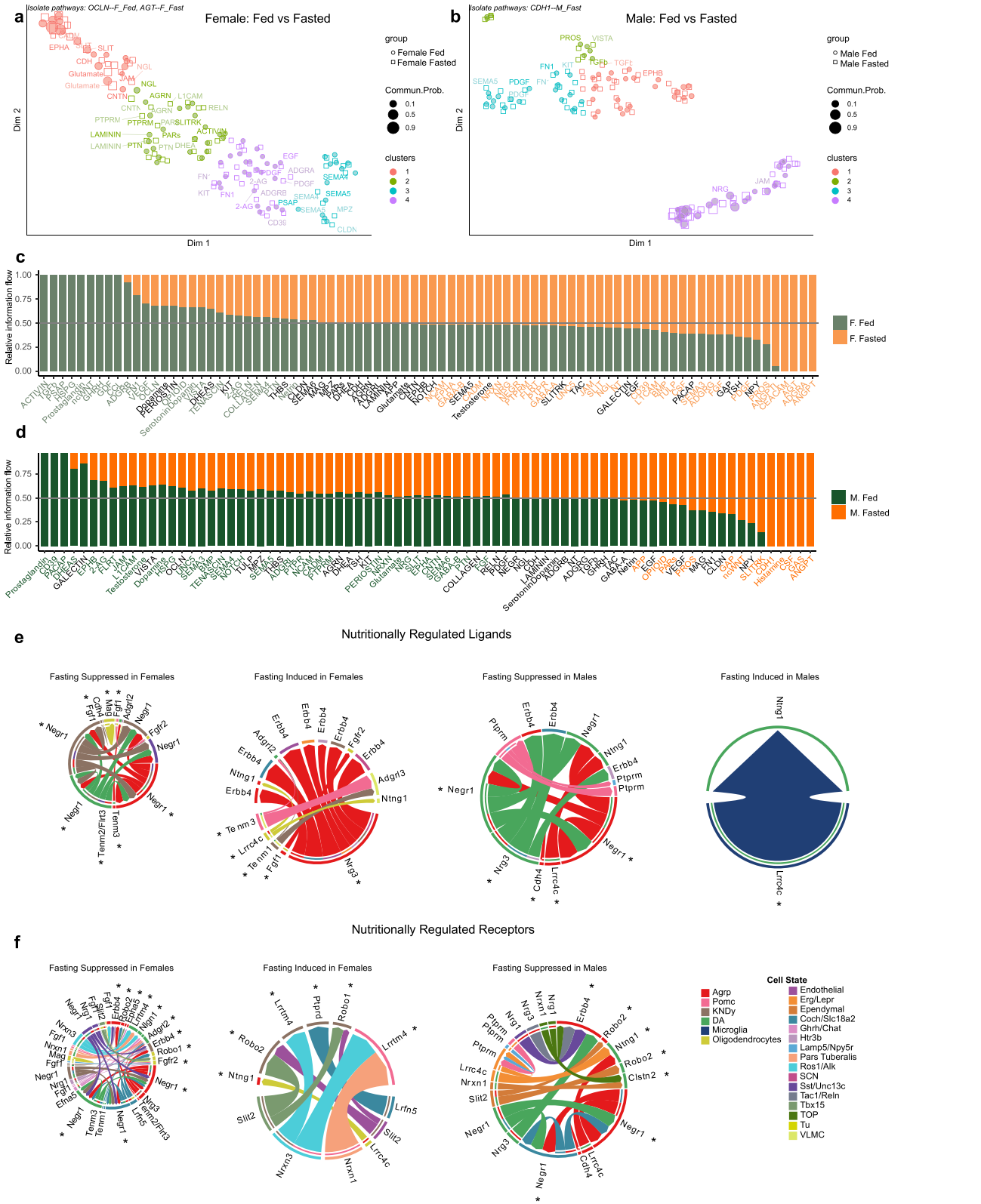

Fig. 6 | Neurotrophic signaling nutritionally regulated in ARH. a, **b** Jointly projecting and clustering signaling pathways for fed and fasted females, **a** or males **b** onto two-dimensional manifold space according to functional similarity of the inferred networks. Each dot or square represents the communication probability. Different colors represent groups of the signaling pathways. **c**, **d** Balance of signaling pathways between fed and fasted females, **c** or males **d**. Significantly different pathways are labeled in color. **e** Chord plots showing DE ligand genes for fed vs fasted in females, left two, and males, right two. **f** Chord plots showing DE receptor genes between fed and fasted in females, left two, and males, right one. M male, F female, DA dopamine, OPC Oligodendrocyte precursor cells, SCN suprachiasmatic nucleus, VLMC vascular leptomeningeal cells, Tu olfactory tubercle, TOP true committed oligodendrocyte progenitor cell.

https://doi.org/10.1038/s41467-026-69239-w

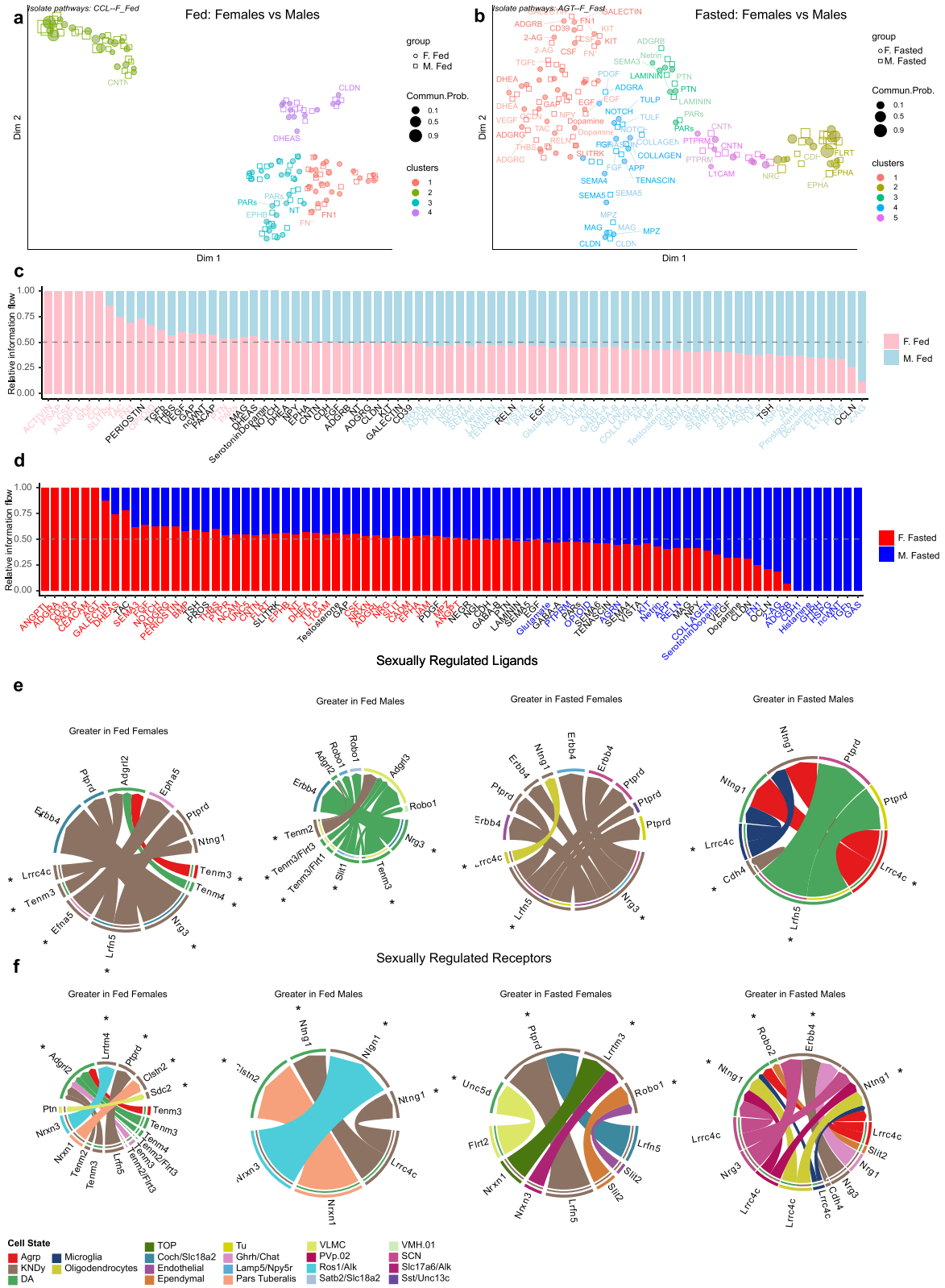

Fig. 7 | Neurotrophic signaling sexually regulated in ARH. a, **b** Jointly projecting and clustering signaling pathways for female and male fed, **a** or fasted mice **b** onto two-dimensional manifold space according to functional similarity of the inferred networks. Each dot or square represents the communication probability. Different colors represent groups of the signaling pathways. **c**, **d** Balance of signaling pathways between female and male fed, **c** or fasted mice **d**. Significantly different pathways are labeled in color. **e** Chord plots showing DE ligand genes for female vs male in fed, left two, and fasted mice, right two. **f** Chord plots showing DE receptor genes between female and male in fed, left two, and fasted, right two. M male, F female, SCN suprachiasmatic nucleus, VLMC vascular leptomeningeal cells, Tu olfactory tubercle, TOP true committed oligodendrocyte progenitor cell, PVp posterior periventricular nucleus.

during the light cycle, when mice are least active and/or sleeping, slowly ramping up in activity as the dark cycle approaches when mice will be active and doing the majority of their feeding[38]. Previous studies have examined ARH cells' response to nutritional state challenges with a focus on Agrp neurons[18,20,39]. Here we find similar results with *Agrp* itself, *Npy*, and *Vgf* induced by fasting and *Rgs6* suppressed by fasting, while finding results of *Fgf1* and *Nrg3* induced by fasting. Differences in results could be due to our approach of euthanizing mice during their active phase at night. While this may be the most physiologically relevant period to study, most groups avoid this period due to the inconvenience it poses to the researchers. A single intracerebroventricular injection of Fgf1 was shown to reverse hyperglycemia in a diabetic model[40]. Agrp neuron overexpression of Fgf1 during fasting is particularly interesting as activation of Agrp neurons increases carbohydrate utilization[41]. To explore broader transcriptional responses in Agrp neurons, we performed co-expression analysis using hdWGCNA. This revealed fasting-induced, female-biased activation of gene modules involved in synaptic signaling and neuropeptide regulation, including one centered around the hub gene *Nrg3*. These findings suggest that fasting elicits coordinated transcriptional reprogramming in Agrp neurons, with particularly strong effects observed in females.

Pomc neurons represent another key ARH population that regulate feeding and metabolism[37]. Pomc neurons had higher expression of *Fos* in the fed condition for both sexes, although only significantly in males. Interestingly, females had many more DEGs related to nutritional regulation. GO:MF revealed that cAMP binding was suppressed by a fast in females while voltage-gated potassium channel activity was induced by a fast in females. Growth hormone receptor activity was higher in fed males than females, while glutamate receptor activity was higher in fasted females than males. While cluster-level analysis indicated an overall feeding-associated activation of Pomc neurons, sub-cluster–level analysis revealed divergent response patterns across Pomc sub-clusters. Pomc/Anxa2 and Pomc/Gipr1 neurons showed minimal *Fos* induction across nutritional states in both sexes, whereas Pomc/Ttr neurons exhibited a pronounced feeding-associated *Fos* increase selectively in females. Together, these findings suggest that the cluster-level Pomc response reflects the combined activity of heterogeneous subpopulations with distinct sex- and nutrition-dependent profiles. Importantly, this sub-cluster–level diversity does not contradict the cluster-level observations but rather provides additional resolution into the cellular complexity underlying Pomc neuron function.

KNDy neurons are a population of neurons located in the ARH that express *Kiss1*, *Tac2* (Neurokinin B), and *Pdyn* (Dynorphin). These neurons along with a second set of *Kiss1*-expressing neurons located in the anteroventral periventricular nucleus (AVPV) help coordinate the release of GnRH from GnRH-expressing neurons. While AVPV Kiss1 neurons influence the preovulatory surge of GnRH and ultimately LH and FSH surges, KNDy neurons are responsible for the pulsatile release of GnRH[16]. Kiss1 neurons have previously been shown to be sensitive to nutritional state alterations via litter size control and even influenced the timing of subsequent puberty onset[38]. Here we show a large number of DEGs present in females after a fast with relatively less seen in the male population. This sexually dimorphic response makes sense in light of the relative cost of reproduction to the sexes[39]. One way that KNDy neurons sense the nutritional state of the animal is through their interconnectedness with Agrp neurons[40]. Although KNDy neurons may express some amount of Lepr, this does not appear to be necessary for Leptin's ability to control puberty timing[41]. GO terms 14-3-3 protein binding, GTPase regulator activity, and cAMP binding suggest greater GPCR activity in the fed state in females. While greater potassium channel regulator activity seen in the fasted condition suggests that KNDy neurons were inhibited by caloric restriction. This is consistent with reduced fertility often seen with caloric restriction[42].

DA neurons of the ARH are primarily responsible for inhibiting prolactin and thus exert control over lactation[28,43]. Nutritional status can have profound affects on milk production and subsequently pup weight. Interestingly, DA was reduced in malnourished mothers compared to control mothers[44]. We also saw a reduction in Th in both females and males in response to fasting. In agreement, the opposite, increase in Th, was seen after high fat diet exposure[45]. As well as being influenced by nutritional state, DA neurons have been shown to exert control of feeding behavior[13]. Here we found that female DA neurons were nutritionally regulated while male DA neurons only had minimal nutritionally regulated DEGs. DA neurons of the ARH were sexually dimorphic in both fed and fasted states with female DA neurons having higher expression of netrin receptor activity while males DA neurons had higher expression of cadherin binding related genes. Netrin receptors are a family of receptors critical for axon guidance and cell migration[46], while cadherins are an integral part of cell-cell adhesion[47]. This suggests that female DA neurons in the ARH are more dynamic with respect to axon guidance and male DA neurons are more stable with cell-cell adhesion molecules playing a larger role.

Microglia are the resident macrophage of the brain and are responsible for clearing debris as well as synaptic remodeling[48]. Microglia in ARH have shown sensitivity to nutritional state in high fat diet studies[49,50]. Here we found that microglia were one of the more dynamic cell types when controlling for sample size. However, its relatively smaller sample made it difficult to find a large number of changes. Nonetheless, we did observe ion channel regulator activity genes were induced by fasting. This is interesting, as membrane depolarization in microglia can lead to phagocytosis[51]. This may indicate that some synaptic remodeling is occurring during prolonged fasting conditions.

Oligodendrocytes are the functional insulation for axons and greatly improve the conductivity efficiency of neurons[52]. Oligodendrocytes in the ARH are sensitive to nutritional state[53]. Consistently, we found that oligodendrocytes were one of the more dynamic cell-types in response to fasting. Major sex differences were not apparent and both sexes saw an increase in ion channel regulator activity genes induced by fasting. This is intriguing, as oligodendrocytes rely on ion channel activity to maintain their functional integrity[54]. This may indicate that certain ARH circuits are undergoing myelination remodeling during different nutritional state challenges.

We noticed that many of the GO:MF terms were related to cell signaling. This led us to perform a cell-cell communication assay using Cellchat[32]. Cellchat revealed neurotrophic factors as major entities controlled by nutritional state in the ARH. Females saw nutritional regulation of *Fgf1* in both Pomc and Agrp neurons. This is interesting as, a single intracerebroventricular injection of Fgf1 has been shown to reverse hyperglycemia in a diabetic model[55] and Fgf1 has been shown to inhibit Agrp neurons[56]. In our results we saw oligodendrocytes as the major recipient of *Fgf1*, expressing *Fgfr2*. The role *Fgf1* plays here is unclear but perhaps it signals to increase myelination of Agrp neurons after a fast to increase their efficiency in signaling. Females also saw an increase in *Nrg3* in Agrp neurons during a fast while males saw *Nrg3* suppressed by fasting in DA neurons. Targets of this signaling were several populations of neurons. This is in agreement with a report of Erbb4 in the ARH although the cell type was not identified there[57]. Deletion of *Erbb4* elsewhere in the hypothalamus increased body weight in mice without effecting their food intake[58]. While it is impossible to be certain, it is likely that Nrgs-Erbb4 signaling plays a critical role in either metabolism or food intake in the ARH as well, and these results were further supported by NicheNet validation.

In order to collect the entire ARH, the inclusion of other nearby brain regions within the MBH is inevitable[18,19]. The majority of neurons could confidently be annotated as belonging to the ARH. As expected, all samples included some amount of contamination from nearby ventromedial hypothalamic nucleus (VMH) and the posterior part of

the periventricular nucleus of the hypothalamus (PVp), which has only more recently been distinguished from the ARH[59,60]. Some but not all samples included contamination from hypothalamus regions slightly further away, i.e., the suprachiasmatic nucleus (SCN) and medial mammillary body (MM), which is a limitation of the current study. We chose a 28 h fasting in order to ensure sufficient food deprivation and the expected change of the nutritional state of the mice; in addition, the extra 4 h beyond the 24 h period were necessary to allow tissue collection during the dark cycle without disrupting animals' circadian clock. We acknowledge that prolonged fasting may cause torpor-like responses and alter gene expression in manners different from short-term fasting, which warrant future investigations.

In summary, we found that various cell types are affected by nutritional state in a sex-dependent manner. Agrp neurons were the most sensitive to fasting with the most nutritional state DEGs but with females showing higher sensitivity than males. KNDy neurons were highly sensitive to nutritional state in females and many sexually dimorphic DEGs were present in both fed and fasted state here, with the majority of those on autosomes. DA neurons showed a similar pattern to KNDy neurons with nutritional state DEGs most prominent in females and many sexually dimorphic DEGs present. Pomc neurons showed moderate numbers of DEGs to nutritional regulation. Among glia cells, both oligodendrocytes and microglia were dynamic in responses to nutritional state.

Methods

Mice

All studies were approved by the institute of animal care and use committee (IACUC) at Baylor College of Medicine (BCM). A total of 36 8-week old C57BL/6 (Jackson labs, 000664) mice (18 males and 18 females) were used in this study. The sample size and statistical analysis methods were planned before our study based on the nature of experiments and our previous experience. Mice were housed in a temperature-controlled (23 °C) environment using a 12 h light and 12 h dark cycle (18:00–06:00). For each sex, mice were divided equally into fed and fasted groups ($N = 9$ per condition per sex). Mice in the fasted group were deprived of food beginning at 18:00 through 22:00 the next day, for a total of 28 hours, while fed mice had ad libitum access to food. All mice were euthanized between 22:00 and 24:00, corresponding to 4–6 h into their active phase. Experimenters were not blind to conditions of mice. Within each condition and sex, three mice were pooled to form one biological replicate, resulting in a total of 12 biological samples (six fed and six fasted). Mice were euthanized in sequential order such that no condition had all mice for that sample collected at the front or back end of the 2 h window. The three batches were collected across three consecutive nights (Supplementary Fig. 1a). Mice were euthanized by placing them in a chamber with isoflurane until all signs of breathing had stopped and perfused with ice-cold saline. Brains were dissected on ice then placed in a brain matrix. Two, one mm sections were taken from Bregma −0.9 to −1.9 and from Bregma −1.9 to −2.9 mm. A one mm harris uni-core was used to take semi-punches from these sections approximately −5.5 to −6.0 mm ventral to Bregma. Tissue was then snap frozen in liquid nitrogen.

Library preparation

Single-nucleus suspensions were prepared following the protocol we described previously[61]. Nuclei were stained by Hoechst-33342 (1:1000; >5 min). Next, we collected nuclei using Fluorescence activated cell sorting (FACS). We used the BD Aria III sorter for collecting nuclei. Hoechst+ nuclei were collected during sorting into a 1.5 ml tube with 200ul 1x PBS with 0.5% BSA as the receiving buffer (RNase inhibitor added). For each 10x Genomics run, 80k–150k nuclei were collected. Nuclei were spun down for 10 min at 800 g at 4 °C, and then resuspended using 30ul of 1x PBS with 0.5% BSA (RNase inhibitor added). 2ul nucleus suspension was used for counting the nuclei with hemocytometers to calculate the concentration. When loading to the 10x controller, we always try to target 10k nuclei for each run. We observed that loading 2 folds more could allow us to recover about 10k cells after sequencing. For example, if we try to target 10k nuclei, we will load 20k into a 10x controller.

Next, 10x Genomics sequencing libraries were prepared following the standard protocol from 10x Genomics 3' v3.1 dual index kit with following settings. All PCR reactions were performed using the Biorad C1000 Touch Thermal cycler with 96-Deep Well Reaction Module. Cycle numbers were used as the 10x protocol recommended for cDNA amplification and sample index PCR. As per 10x protocol, 1:10 dilutions of amplified cDNA and final libraries were evaluated on Agilent TapeStation.

Libraries were then shipped on dry ice to Novogene (Sacramento, CA) for sequencing. Fastqs were downloaded from Novogene's website. Fastqs were aligned to Mus musculus genome assembly GRCm39 using STAR solo 2.7.10b using options soloFeatures set to GeneFull_Ex50pAS and soloCellFilter set to EmptyDrops_CR. Output was then loaded into R 4.4.0. Code can be found at: https://github.com/jbeanphd/ARH_Sex_by_Nutr/blob/main/starsolo.sh.

Bioinformatics

Ambient RNA was estimated and removed using SoupX 1.6.2 using adjustCounts method set to "multinomial". Potential doublets were identified and removed using scDblFinder 1.17.3. Cells with extreme values for counts, mitochondrial percent, ribosomal protein percent, and hemoglobin counts were filtered out using mean + 4 s.d. as a threshold. Code can be found at: https://github.com/jbeanphd/ARH_Sex_by_Nutr/blob/main/SoupX_scDblFnd.R.

Data were analyzed using Seurat 5.0.3[62]. Counts were normalized using SCTransform() function with do.scale and do.center set to false. Mitochondrial, ribosomal proteins, and hemoglobin genes were excluded from variable genes. PCA was performed on the variable features. T-distributed stochastic neighbor embedding was estimate for the 1st 30 PCs. Cluster were determined using FindNeighbors() and FindClusters() functions with resolution set to 0.8 to distinguish neurons from major glia types and to 1.5 to distinguish neuron subtypes. FindAllMarkers() function was used to find marker genes for each cluster. Marker genes were then used to annotate cell-types. Data from GSE90806[18] were used as reference for annotation. Marker genes were determined for GSE90806 and overlap was calculated and the closest correlation was used to annotate the cell-types if the annotating genes were included in the current studies marker genes. If not one to two genes with the largest log2 fold-change were used to annotate the cell-type. ARH neurons are a heterogeneous population. In order to ensure the most accurate annotation of ARH neurons, we reclustered nuclei belonging to this category at a higher resolution. ARH neurons formed 18 unique clusters (Fig. 1d). We annotated these clusters using genes that showed the largest fold-change and largest percent expressed differences between the neurons within each cluster and those outside of the given cluster (Fig. 1d; Supplementary Fig. S3). Code can be found at: https://github.com/jbeanphd/ARH_Sex_by_Nutr/blob/main/Annotation.R

Fos expression levels were quantified from the SCT-normalized assay within the Seurat object. Expression values for *Fos* were extracted from the normalized data matrix (SCT@data) and merged with the corresponding metadata (sex and nutritional state) for downstream visualization. Bar plots of *Fos* expression were generated using the ggplot2 package, summarizing data as mean ± SEM for each experimental group (n = 3 biological replicates per condition). Statistical significance between groups was assessed using the Wilcoxon rank-sum test, followed by Bonferroni correction for multiple comparisons Code can be found at: https://github.com/jbeanphd/ARH_Sex_by_Nutr/blob/main/isolate_cell_types.R.

For IEGs analysis, DE analyses were conducted using FindMarkers() function with the Wilcoxon rank-sum test, comparing groups across four sex and nutritional states. IEGs expression levels were visualized using Z-score-scaled heatmaps. To assess differential responsiveness, volcano plots were generated displaying average log2 fold change against adjusted p values. Code can be found at: https://github.com/jbeanphd/ARH_Sex_by_Nutr/blob/main/isolate_cell_types.R.

Differential expression was calculated using the function FindMarkers() with logfc.threshold set to log2 (1.25), min.pct set to 0.25 pseudocount.use set to 1, test.use set to MAST, and latent.variable set to Sample_ID. Conditions were tested pairwise: female fed vs fasted, male fed vs fasted, fed female vs male, and fasted female vs male. Code can be found at: https://github.com/jbeanphd/ARH_Sex_by_Nutr/blob/main/Differential_expression.R.

To mitigate potential batch effects in some cell types across different conditions, we performed integration using the RPCA workflow in Seurat. The dataset was first split by batch, and each subset was independently normalized and processed to identify 2000 highly variable genes using the "vst" method. Shared variable features across batches were selected and used to scale the data and perform PCA within each subset. Integration anchors were then identified using the function FindIntegrationAnchors(), and datasets were integrated using IntegrateData(). The integrated object was scaled and used for dimensionality reduction, and clustering. In addition, we integrated our neuronal dataset with the data from GSE9080618 (neurons only), using the same method described above. Code can be found at: https://github.com/jbeanphd/ARH_Sex_by_Nutr/blob/main/RPCA.R.

Cell-cell communication was accessed using CellChat 2.1.2[32]. Functions: identifyOverExpressedGenes, identifyOverExpressedInteractions, computeCommunProb, computeCommunProbPathway, aggregateNet, and netAnalysis_computeCentrality were used for the initial analyses. Functions computeNetSimilarityPairwise, netEmbedding, netClustering, and netVisual_embeddingPairwise were used to visualize signaling pathway similarity in reduced dimensionality. Chord plots were generated using netVisual_chord_gene. Code can be found at: https://github.com/jbeanphd/ARH_Sex_by_Nutr/blob/main/CellChat.R.

To validate the potential ligand–receptor interactions predicted by Cellchat, we performed complementary analysis using NicheNet 2.2.0[63]. Potential ligands were defined based on our Cellchat results, and expressed genes were filtered using a minimum expression threshold across cells within each cell type. For each receiver cell type, we identified DEGs between conditions (fasting vs. fed or female vs. male) using the function FindMarkers in Seurat, with logfc.threshold set to log2 (1.25). These DEGs were used as the target gene set in NicheNet's predict_ligand_activities() function to estimate the ligand regulatory potential. Potential ligands were ranked based on corrected Pearson correlation between ligand regulatory potential scores and observed gene expression patterns. Specifically, we used the get_weighted_ligand_receptor_links() function to extract ligand–receptor pairs between the given ligands and the expressed receptors in the receiver cell population. The resulting ligand–receptor interaction matrix was then visualized using hierarchical clustering and heatmap plotting with prepare_ligand_receptor_visualization() and make_heatmap_ggplot(), highlighting the potential binding landscape between sender-derived ligands and receiver-expressed receptors. Code can be found at:/ https://github.com/jbeanphd/ARH_Sex_by_Nutr/blob/main/NicheNet.R.

We applied the R package hdWGCNA 0.4.05[64] to identify gene co-expression modules within Agrp neurons. Metacells were constructed to reduce noise, and genes with low expression or variability were filtered out. A signed network was built using soft-thresholding to approximate scale-free topology, followed by hierarchical clustering to define gene modules. Module eigengenes (MEs) were calculated, and DME analysis was performed to assess module-level changes across nutritional and sex conditions. Hub genes were identified based on intramodular connectivity, and functional enrichment was performed for selected modules. All parameters were set as default. Code can be found at: https://github.com/jbeanphd/ARH_Sex_by_Nutr/blob/main/hdWGCNA.R.

RNAscope

Eight-week old C57BL/6 mice were either ad libitum fed or were fasted from 18:00 to 22:00 the next day for a total of 28 h. Experimenters were not blind to conditions of mice. Mice were anesthetized and perfused transcardially with 0.9% saline followed by 10% formalin. Brains were removed and post fixed in 10% formalin for 16 h at 4 °C and cryoprotected in 30% sucrose for 48 h. Brains were frozen, sectioned at 15 μm using the cryostat collected into six separate series, washed in DEPC-treated phosphate buffered saline (PBS) for 10 minutes. Sections were mounted on DEPC-treated charged slides, dried for 0.5 h at room temperature and stored at −80 °C. On the day of the RNAScope assay, the slides were thawed and rinsed two times in 1X PBS and placed in an oven for 30 min at 60 °C. After that, slides were post fixed in 10% formalin for 20 min at 4 °C. Slides were then gradually dehydrated in ethanol (50, 70 and 100%, 5 min each) and underwent target retrieval for 5 minutes at 100 °C. Slides were incubated in protease III (#322337, ACDBio) for 30 min at 40 °C. Slides were then rinsed in distilled water and incubated in RNAscope probes for Agrp (#400711-C2, ACDBio), *Fgf1* (#466661-C4, ACDBio), and *Rgs6* (#521211 ACDBio) or Tac2 (#446391-C2, ACDBio), *Cntn5* (#567461-C3, ACDBio) and *Tmem266* (#519221, ACDBio) for 2 hours at 40 °C. Sections were then processed using the RNAscope Multiplex Fluorescent Reagent Kit v2 (#323100, ACDBio) according to the manufacturer instructions. Slides were cover-slipped and analyzed using a fluorescence microscope.

Four mice per condition with 3–6 sections per mouse between −1.34 and −1.94 mm respective to the bregma were utilized for analysis. Within each section, 35–78 neurons were analyzed. Agrp or Tac2 neurons were identified and areas were calculated using Qupath v0.6.0. *Fgf1* and *Rgs6* for Agrp neurons or *Cntn5* and *Tmem266* for Tac2 neurons were calculated as a percentage of respective neurons.

Reporting summary

Further information on research design is available in the Nature Portfolio Reporting Summary linked to this article.

Data availability

The fully processed snRNA-seq dataset generated in this study have been deposited in the Gene Expression Omnibus (GEO) database under accession code GSE282955. Source data are provided as a Source Data file. Source data are provided with this paper.

Code availability

Detailed analysis codes used in this study are available on the Github repository 663 (https://github.com/jbeanphd/ARH_Sex_by_Nutr) https://doi.org/10.5281/zenodo.18276251.

References

1. World Health Organization. *World Health Statistics 2023: Monitoring Health for the SDGs, Sustainable Development Goals*. 1–119 https://www.who.int/publications-detail-redirect/9789240074323 (WHO, 2023).
2. Bryan, S. et al. *NHSR 158. National Health and Nutrition Examination Survey 2017–March 2020 Pre-Pandemic Data Files*. https://stacks.cdc.gov/view/cdc/106273 (NHSR, 2021) https://doi.org/10.15620/cdc:106273.
3. Collaboration, P. S Body-mass index and cause-specific mortality in 900 000 adults: collaborative analyses of 57 prospective studies. *Lancet* **373**, 1083–1096 (2009).

4. Kannel, W. B. et al. Regional obesity and risk of cardiovascular disease; the Framingham study. *J. Clin. Epidemiol.* **44**, 183–190 (1991).
5. Gesta, S., Tseng, Y.-H. & Kahn, C. R. Developmental origin of fat: tracking obesity to its source. *Cell* **131**, 242–256 (2007).
6. Lee, C. G. et al. Adipokines, inflammation, and visceral adiposity across the menopausal transition: a prospective study. *J. Clin. Endocrinol. Metab.* **94**, 1104–1110 (2009).
7. Xu, Y. et al. Distinct hypothalamic neurons mediate estrogenic effects on energy homeostasis and reproduction. *Cell Metab.* **14**, 453–465 (2011).
8. Wislocki, G. B. & King, L. S. The permeability of the hypophysis and hypothalamus to vital dyes, with a study of the hypophyseal vascular supply. *Am. J. Anat.* **58**, 421–472 (1936).
9. Gross, P. M. & Weindl, A. Peering through the windows of the brain. *J. Cereb. Blood Flow. Metab. J. Int. Soc. Cereb. Blood Flow. Metab.* **7**, 663–672 (1987).
10. Zhang, Y. et al. Positional cloning of the mouse obese gene and its human homologue. *Nature* **372**, 425–432 (1994).
11. Castro-Dufourny, I., Carrasco, R., Prieto, R. & Pascual, J. M. Jean Camus and Gustave Roussy: pioneering French researchers on the endocrine functions of the hypothalamus. *Pituitary* **20**, 409–421 (2017).
12. Krashes, M. J. et al. Rapid, reversible activation of AgRP neurons drives feeding behavior in mice. *J. Clin. Invest.* **121**, 1424–1428 (2011).
13. Zhang, X. & van den Pol, A. N. Hypothalamic arcuate nucleus tyrosine hydroxylase neurons play orexigenic role in energy homeostasis. *Nat. Neurosci.* **19**, 1341–1347 (2016).
14. Fenselau, H. et al. A rapidly acting glutamatergic ARC→PVH satiety circuit postsynaptically regulated by α-MSH. *Nat. Neurosci.* **20**, 42–51 (2017).
15. Zhan, C. et al. Acute and long-term suppression of feeding behavior by POMC neurons in the brainstem and hypothalamus, respectively. *J. Neurosci. J. Soc. Neurosci.* **33**, 3624–3632 (2013).
16. Herbison, A. E. Control of puberty onset and fertility by gonadotropin-releasing hormone neurons. *Nat. Rev. Endocrinol.* **12**, 452–466 (2016).
17. Thorner, M. O. et al. Physiological role of somatostatin on growth hormone regulation in humans. *Metabolism* **39**, 40–42 (1990).
18. Campbell, J. N. et al. A molecular census of arcuate hypothalamus and median eminence cell types. *Nat. Neurosci.* **20**, 484–496 (2017).
19. Deng, G. et al. Single-nucleus rna sequencing of the hypothalamic arcuate nucleus of C57BL/6J mice after prolonged diet-induced obesity. *Hypertens. Dallas Tex.* **76**, 589–597 (2020).
20. Steuernagel, L. et al. HypoMap—a unified single-cell gene expression atlas of the murine hypothalamus. *Nat. Metab.* **4**, 1402–1419 (2022).
21. Germain, P.-L., Lun, A., Garcia Meixide, C., Macnair, W. & Robinson, M. D. Doublet identification in single-cell sequencing data using scDblFinder. *Research* **10**, 979 (2021).
22. Li, H. et al. Fly cell atlas: a single-nucleus transcriptomic atlas of the adult fruit fly. *Science* **375**, eabk2432 (2022).
23. Lu, T.-C. et al. Aging fly cell atlas identifies exhaustive aging features at cellular resolution. *Science* **380**, eadg0934 (2023).
24. Luecken, M. D. & Theis, F. J. Current best practices in single-cell RNA-seq analysis: a tutorial. *Mol. Syst. Biol.* **15**, e8746 (2019).
25. Young, M. D. & Behjati, S. SoupX removes ambient RNA contamination from droplet-based single-cell RNA sequencing data. *GigaScience* **9**, giaa151 (2020).
26. MAST: a flexible statistical framework for assessing transcriptional changes and characterizing heterogeneity in single-cell RNA sequencing data | Genome Biology | Full Text. https://genomebiology.biomedcentral.com/articles/10.1186/s13059-015-0844-5in/hdWGCNA.R.
27. Luquet, S., Perez, F. A., Hnasko, T. S. & Palmiter, R. D. NPY/AgRP neurons are essential for feeding in adult mice but can be ablated in neonates. *Science* **310**, 683–685 (2005).
28. van Maanen, J. H. & Smelik, P. G. Depletion of monoamines in the hypothalamus and prolactin secretion. *Acta Physiol. Pharmacol. Neerl.* **14**, 519–520 (1967).
29. Tullai, J. W. et al. Immediate-early and delayed primary response genes are distinct in function and genomic architecture. *J. Biol. Chem.* **282**, 23981–23995 (2007).
30. Jurgens, H. A. & Johnson, R. W. Dysregulated neuronal-microglial cross-talk during aging, stress and inflammation. *Exp. Neurol.* **233**, 40–48 (2012).
31. Cai, Z. & Xiao, M. Oligodendrocytes and Alzheimer's disease. *Int. J. Neurosci.* **126**, 97–104 (2016).
32. Jin, S. et al. Inference and analysis of cell-cell communication using CellChat. *Nat. Commun.* **12**, 1088 (2021).
33. Alhadeff, A. L. et al. A neural circuit for the suppression of pain by a competing need state. *Cell* **173**, 140–152 (2018).
34. Burnett, C. J. et al. Hunger-driven motivational state competition. *Neuron* **92**, 187–201 (2016).
35. Dietrich, M. O., Zimmer, M. R., Bober, J. & Horvath, T. L. Hypothalamic AGRP neurons drive stereotypic behaviors beyond feeding. *Cell* **160**, 1222–1232 (2015).
36. Padilla, S. L. et al. Agouti-related peptide neural circuits mediate adaptive behaviors in the starved state. *Nat. Neurosci.* **19**, 734–741 (2016).
37. Xu, Y., Elmquist, J. K. & Fukuda, M. Central nervous control of energy and glucose balance: focus on the central melanocortin system. *Ann. N. Y. Acad. Sci.* **1243**, 1–14 (2011).
38. Castellano, J. M. et al. Early metabolic programming of puberty onset: impact of changes in postnatal feeding and rearing conditions on the timing of puberty and development of the hypothalamic kisspeptin system. *Endocrinology* **152**, 3396–3408 (2011).
39. Navarro, V. M. Metabolic regulation of kisspeptin—the link between energy balance and reproduction. *Nat. Rev. Endocrinol.* **16**, 407–420 (2020).
40. Padilla, S. L. et al. AgRP to Kiss1 neuron signaling links nutritional state and fertility. *Proc. Natl. Acad. Sci. USA* **114**, 2413–2418 (2017).
41. Donato, J. et al. Leptin's effect on puberty in mice is relayed by the ventral premammillary nucleus and does not require signaling in Kiss1 neurons. *J. Clin. Invest.* **121**, 355–368 (2011).
42. Sun, J. et al. Caloric restriction in female reproduction: is it beneficial or detrimental? *Reprod. Biol. Endocrinol.* **19**, 1 (2021).
43. Caron, M. G. et al. Dopaminergic receptors in the anterior pituitary gland. Correlation of [3H]dihydroergocryptine binding with the dopaminergic control of prolactin release. *J. Biol. Chem.* **253**, 2244–2253 (1978).
44. Manjarrez-Gutiérrez, G., González-Ramírez, M., de Oca, A. B.-M., Herrera-Márquez, R. & Hernández-Rodríguez, J. Serotonin and dopamine in the hypothalamus of control and malnourished mother rats during pregnancy and lactation and body composition of their offspring. *Nutr. Neurosci.* **16**, 225–232 (2013).
45. Lee, A. K. et al. Effect of high-fat feeding on expression of genes controlling availability of dopamine in mouse hypothalamus. *Nutrition* **26**, 411–422 (2010).
46. Moore, S. W., Tessier-Lavigne, M. & Kennedy, T. E. Netrins and their receptors. *Adv. Exp. Med. Biol.* **621**, 17–31 (2007).
47. Cavallaro, U. & Christofori, G. Cell adhesion and signalling by cadherins and Ig-CAMs in cancer. *Nat. Rev. Cancer* **4**, 118–132 (2004).
48. Wu, Y., Dissing-Olesen, L., MacVicar, B. A. & Stevens, B. Microglia: dynamic mediators of synapse development and plasticity. *Trends Immunol.* **36**, 605–613 (2015).
49. Huang, Y. et al. Maternal dietary fat during lactation shapes single nucleus transcriptomic profile of postnatal offspring hypothalamus

in a sexually dimorphic manner in mice. *Nat. Commun.* **15**, 2382 (2024).
50. Thaler, J. P. et al. Obesity is associated with hypothalamic injury in rodents and humans. *J. Clin. Invest.* **122**, 153–162 (2012).
51. Lv, Z. et al. Clearance of β-amyloid and synapses by the optogenetic depolarization of microglia is complement selective. *Neuron* **112**, 740–754 (2024).
52. Nave, K.-A. & Werner, H. B. Myelination of the nervous system: mechanisms and functions. *Annu. Rev. Cell Dev. Biol.* **30**, 503–533 (2014).
53. Kohnke, S. et al. Nutritional regulation of oligodendrocyte differentiation regulates perineuronal net remodeling in the median eminence. *Cell Rep.* **36**, 109362 (2021).
54. Saab, A. S. et al. Oligodendroglial NMDA receptors regulate glucose import and axonal energy metabolism. *Neuron* **91**, 119–132 (2016).
55. Scarlett, J. M. et al. Peripheral mechanisms mediating the sustained antidiabetic action of FGF1 in the brain. *Diabetes* **68**, 654–664 (2019).
56. Hwang, E. et al. Sustained inhibition of NPY/AgRP neuronal activity by FGF1. *JCI Insight* **7**, e160891 (2022).
57. Bean, J. C. et al. Genetic labeling reveals novel cellular targets of schizophrenia susceptibility gene: distribution of GABA and non-GABA ErbB4-positive cells in adult mouse brain. *J. Neurosci.* **34**, 13549–13566 (2014).
58. Santiago-Marrero, I. et al. Energy expenditure homeostasis requires ErbB4, an obesity risk gene, in the paraventricular nucleus. *eNeuro* **10**, 0139 (2023).
59. Paxinos, G. & Franklin, K. B. J. *The Mouse Brain in Stereotaxic Coordinates*. (Academic Press, 2001).
60. Lein, E. S. et al. Genome-wide atlas of gene expression in the adult mouse brain. *Nature* **445**, 168–176 (2007).
61. McLaughlin, C. N., Qi, Y., Quake, S. R., Luo, L. & Li, H. Isolation and RNA sequencing of single nuclei from *Drosophila* tissues. *STAR Protoc.* **3**, 101417 (2022).
62. Butler, A., Hoffman, P., Smibert, P., Papalexi, E. & Satija, R. Integrating single-cell transcriptomic data across different conditions, technologies, and species. *Nat. Biotechnol.* **36**, 411–420 (2018).
63. Browaeys, R., Saelens, W. & Saeys, Y. NicheNet: modeling intercellular communication by linking ligands to target genes. *Nat. Methods* **17**, 159–162 (2020).
64. Morabito, S., Reese, F., Rahimzadeh, N., Miyoshi, E. & Swarup, V. hdWGCNA identifies co-expression networks in high-dimensional transcriptomics data. *Cell Rep. Methods* **3**, 100498 (2023).

Acknowledgements

H.L. discloses support for the research of this work from the CPRIT Scholar in Cancer Research [RR200063], NIH/NIA [U01AG086143], NIH [DP2AT013275], the Longevity Impetus Grant, the Ted Nash Long Life Foundation, and the Welch Foundation. Y.X. discloses support for the research of this work from the Silver Endowment. X.F. discloses support for the research of this work from NIDDK [1F32DK138685-01A1]. M.W. discloses support for the research of this work from NIMHD [1F32HD112123-01A1].

Author contributions

J.C.B., H.L., and Y.X. co-conceptualized the study. J.C.B. and J.J. performed the experiments and analyses, with assistance from T.C.L., H.L., K.M.M., D.A.T., S.V.J., M.E.B., J.C., Y.D., X.F., X.G., J.H., Y.L., H.L., Q.L., Y.L., Y.S., L.T., M.W., X.X., Y.Y., M.Y., X.L., M.S., F.W., O.Z.G., Y.Y., Y.H., C.W., and Y.Q., H.L., and Y.X. supervised the study.

Competing interests

The authors declare no competing interests.

Additional information

Supplementary information The online version contains supplementary material available at https://doi.org/10.1038/s41467-026-69239-w.

Correspondence and requests for materials should be addressed to Hongjie Li or Yong Xu.

Peer review information *Nature Communications* thanks Tune Pers and the other, anonymous, reviewer(s) for their contribution to the peer review of this work. A peer review file is available.